NJC

Accepted Manuscript

This is an *Accepted Manuscript*, which has been through the Royal Society of Chemistry peer review process and has been accepted for publication.

Accepted Manuscripts are published online shortly after acceptance, before technical editing, formatting and proof reading. Using this free service, authors can make their results available to the community, in citable form, before we publish the edited article. We will replace this *Accepted Manuscript* with the edited and formatted *Advance Article* as soon as it is available.

You can find more information about *Accepted Manuscripts* in the Information for Authors.

Please note that technical editing may introduce minor changes to the text and/or graphics, which may alter content. The journal's standard Terms & Conditions and the Ethical guidelines still apply. In no event shall the Royal Society of Chemistry be held responsible for any errors or omissions in this *Accepted Manuscript* or any consequences arising from the use of any information it contains.

ROYAL SOCIETY OF CHEMISTRY

www.rsc.org/njc

Controlled synthesis of CoO/C and Co/C nanocomposites via molten salt method and their lithium-storage properties

Shasha Chu[a], Chao Yang[a], Xin Xia[c] Jide Wang[a], Yanglong Hou[b], Xintai Su[a]*

[a] *Ministry Key Laboratory of Oil and Gas Fine Chemicals, College of Chemistry and Chemical Engineering, Xinjiang University, Urumqi 830046, China.*

[b] *Department of Materials Science and Engineering College of Engineering, Peking University, Beijing 100871, China.*

[c.] *College of Textile and Clothing, Xinjiang University, Urumqi 830046, China.*

[a*] Corresponding author. Tel. & fax: +86 991 8581018.

E-mail address: suxintai827@163.com (X. Su)

Abstract

We report a facile molten salt approach to fabricate CoO and Co nanoparticles, which homogeneously embedded in two-dimensional (2D) amorphous carbon nanosheets as an advanced anode materials for high-performance lithium-ion batteries (LIBs). With the aid of Na_2SO_4 particles, the ultra-small CoO/C or Co/C hybrid nanocomposites were synthesized simultaneously through a single heating procedure using $Co(OH)_2$@OA complex as the precursors for both CoO(Co) and thin carbon layers. The hybrid nanocomposites (C500, C600) exhibited an unexpected initial discharge capacity of 1618.2 and 873 mA h g^{-1} and high reversible specific capacity (642.1 and 500 mA h g^{-1} over 50 cycles at 70 mA g^{-1}). The design of ultrafine CoO (Co) nanoparticles encapsulated with thin carbon layers can not only achieve long cycle life, but also effectively avoid the particle cracking, pulverization and aggregation upon cycling. Moreover, the findings open new paths for the

exploiting of advanced active materials and electrolytes for Li ion batteries and other energy storage devices.

1. Introduction

Rechargeable lithium-ion batteries (LIBs) have been most intensively used in hybrid electric vehicles (HEVs) and electric vehicles (EVs).[1-5] An increased research effort is urgently required to develop flexible rechargeable LIBs with large capacity, high power, and long cycling life.[6-10] Energy density, durability and costs are also the most concerned issues in the battery research.[11-14] Currently, the traditional graphite negative electrode material has already reached its theoretical limit (372 mA h g-1).[3, 15-17] As alternative anode materials to graphite, some transition metals or their oxide, such as Co and CoO, [18, 19] have attracted the attention due to their quite high theoretical capacity (~1000 mA h g^{-1}).[20-23] However, low electrical conductivity and poor mechanical stability have limited their applications as LIB electrode materials.[24] Consequently, a key issue is how to improve the charge transport and mechanical durability of the anode materials.

In order to overcome the above problems, a promising strategy is to construct hybrid electrodes composed of MO_x and carbon on the nanoscale.[25, 26] Moreover, coating a carbon layer on the surface of MO_x nanoparticles can also prevent the particles from aggregating and reduce the side reactions at the interface between MO_x and electrolyte.[11, 17, 27] A series of MO_x/carbon hybrids,

such as carbon-coated MO_x nanostructures, MO_x-decorated graphene, or MO_x-anchored carbon nanosheets hybrids have been extensively reported.[23, 28-33] These MO_x/carbon hybrid electrodes have been demonstrated to provide a large space available to accommodate volume change during the lithiation and delithiation processes and maintain the mechanical integrity of the composite electrode.[34] A rational design of MO_x/carbon hybrid can not only improve the cycling performance of the MO_x-based anodes, but also enhance the high rate performance of the battery.[35-37] Therefore, it is still desirable to design novel MO_x/carbon-based anode materials with longer cycling life and higher rate performance.

Herein, we present a facile method for the preparation of ultra-small CoO/Co nanoparticles encapsulated with thin carbon layers by using inorganic salt (Na_2SO_4) as the template. The ultra-small CoO nanoparticles and Co nanoparticles are anchored strongly onto the carbon nanosheet through the thermal decomposition of $Co(OH)_2$@OA precursor. The electrochemical performance of CoO/C and Co/C nanocomposites as a negative electrode material for LIBs was studied and showed outstanding enhancement of cycle performance (with ~99% capacity retention over 50 cycles) and reversible specific capacity (642.1 and 500 mA h g^{-1} over 50 cycles at 70 mA g^{-1}). We proposed a possible origin of the reversible capacity of metallic Co nanoparticles on the reversible formation/decomposition in solid electrolyte interface films, which gives a further understanding for the role of the

transition-metal nanoparticles in lithium storage. Furthermore, this work is very helpful to enlighten us on exploiting advanced materials for Li ion batteries and other energy storage devices.

2. Experimental

All of the chemical reagents were of pure analytical grade and were used without further purification.

2.1 Preparation of CoO/C and Co/C nanocomposites

In a typical preparation procedure, 2 mmol of sodium oleate was dispersed in 10 mL of 0.1 M $Co(NO_3)_2$ aqueous solution, and then mixed with 20 mL of ethanol and 30 mL of hexane with the aid of ultrasonic. The solution was heated to 70^{o}C and mixed completely using a magnetic stirrer in a closed container placed in oil bath. 2 mmol of KOH were added into the solution after stirred for 30 min, simultaneously, the suspension was heated at 70^{o}C for another 8 h. The complex was collected by centrifugation and washed with deionized water and ethanol several times, and then dried at 80^{o}C for 12 h. The obtained brownish $Co(OH)_2$@OA precursor mixed with a mass of Na_2SO_4 and ground in a mortar to form a homogeneous powder. The mixtures were sintered at 350, 400, 500 and 600^{o}C for 3 h (with a heating rate of 10^{o}C min^{-1} and the gas flow rate of Ar was fixed at 0.04 slpm) and allowed to cool naturally. After being cooled to room temperature, the product was washed with deionized water and ethanol for three times, followed by drying at 80^{o}C for 6 h.

2.2 Characterization

The crystal structure of the samples was determined by X-ray diffraction (XRD) using a BRUKER D2 X-ray diffractometer over with Cu Kα radiation (λ=1.54178 Å). The scanning angle was between the 2θ ranging from 10° to 70° with a scanning rate of 2° min^{-1}. X-ray photoelectron spectroscopy (XPS) analyses were performed in an AXIS Nova (Kratos Inc., UK) with hemispherical energy analyzer using monochromatic light. The content of Co in CoO/C nanocomposites were determined by inductively coupled plasma (ICP) analysis on a Perkin-Elmer OPTIMA 3000-XL ICP emission spectrometer. Thermogravimetric analysis (TGA) was measured on an SDT Q600 V20.9 Build 20. The morphologies and microstructures of the samples were characterized by Transmission electron microscopy (TEM, JEOL-1011) and scanning electron microscope (SEM, Hitachi S4800). Fourier transform infrared (FT-IR) spectra were collected with a BRUKER EQUINOX55 spectrophotometer in the wave number interval between 4000 and 400 cm^{-1}.

2.3 Electrochemical measurement

The working electrodes were made through the following steps: active materials (CoO/C nanocomposites or Co/C nanocomposites), conductivity agent (carbon black), and binder (polytetrafluoroethene, PTFE) in a weight ration of 80:10:10 were blended with ethanol as solvent. Then the electrodes were cut into disks and dried at 100°C for 24 h under vacuum. Lithium foil was used as the counter and reference electrode, and polypropylene (PP) membrane (Celgard 2400) was employed as a separator. The cell were assembled in a

glove box (Mbraun, labstar, Germany) and the electrolyte solution was a 1 M solution of $LiPF_6$ in ethylene carbonate (EC), diethyl carbonate (DEC) and methyl carbonate (DMC) (1:1:1, v/v/v). The charge/discharge test were carried out on a LAND CT2001A test system between 0.01 and 3.0 V (vs. Li/Li^+) at a current density of 70 mA g^{-1} at room temperature. Cyclic voltammetry (CV) measurement was carried out using LK2005 electrochemical workstation at a scanning rate of 0.1 mV s^{-1}. The batteries were assembled in an argon-filled glovebox and galvanostatic charged/discharged at current densities of 70 mA g^{-1} in the fixed voltage range of 0.01-3.0 V at room temperature.

3. Results and discussion

3.1. Growth mechanism of the CoO/C and Co/C nanocomposites

The schematic for the preparation of CoO/C and Co/C nanocomposites is displayed in Scheme 1. The inorganic-organic [$Co(OH)_2$@OA] precursor are synthesized via a two-phase procedure with sodium oleate as the structure-directing agent (The XRD result shows that the precursor is $Co(OH)_2$@OA, Fig. S1). Firstly, $Co(NO_3)_2 \cdot 6H_2O$, KOH and sodium oleate were reacted in the water/ethanol/hexane mixture, and $Co(OH)_2$@OA was generated in the up layer. Secondly, the resulting inorganic-organic complex was dried and grinded with Na_2SO_4 to obtain a solid mixture. During the subsequent annealing process in Ar atmosphere at 350, 400 and 500^oC, the as-obtained CoO nanoparticles were converted from $Co(OH)_2$ decomposition, while conductive carbon layers were converted from OA^- carbonization. When

the calcining temperature was increased to 600°C, the CoO nanoparticles were reduced by the carbon layers. The Fourier transform infrared (FT-IR) spectrum of the $Co(OH)_2$@OA complex confirms the adsorption of oleic acid onto the surface of the $Co(OH)_2$ nanoparticles (Fig. S2a). The decomposition process of the inorganic-organic precursor ($Co(OH)_2$@OA) was analyzed by TGA (Fig. S2b). There is no significant weight loss after 600°C, which suggested the complete decomposition of oleic acid. Moreover, the design of ultrafine CoO or Co nanoparticles supported by carbon layer can effectively avoid the particles cracking, pulverization and aggregation upon cycling.

3.2. Structural analysis of CoO/C and Co/C nanocomposites

Fig. 1 shows the X-ray diffraction (XRD) patterns of the as-synthesized products prepared at 350, 400, 500 and 600°C, which are marked as C350, C400, C500 and C600, respectively. It can be seen that all of the diffraction peaks (C350, C400 and C500) can be indexed to the cubic phase of CoO (JCPDS No. 78-0431). No other crystalline impurities are detected, demonstrating the phase purity of the products. However, when the calcination temperature increased to 600°C, $Co(OH)_2$@OA precursor decomposed to cobalt as confirmed by XRD (Fig. 1, C600, JCPDS No. 15-0806). All the products show broader peaks with less intensity, suggesting that the nanocomposites are composed of small particles with relatively low crystallization. The lower intensity may be attributed to the high density of the amorphous carbon wrapped on the surface of CoO and Co nanoparticles to hinder diffusion.[36]

3.3. Composition and morphology analysis of CoO/C nanocomposites

The XPS spectra of CoO/C in Fig. 2a exhibit three main peaks at 284.66, 530.68 and 780.68 eV, corresponding to the peaks of C 1s, O 1s and Co 2p.[32,49] The Co 2p peak is further examined by high-resolution XPS (Fig. 2(b-d)). In the Co 2p region (Fig. 2b), two main peaks with obvious statellite peaks (statellites: 785.4 and 805.4 eV) corresponding to the Co 2p3/2 (780.8 eV) and Co 2p1/2 (796.6 eV) levels are observed, and those two highly intense peaks and the statellites near them is consistent with the presence of Co^{2+} in the high-spin state. The absence of a signal at 778.1 eV indicates the nonexistence of Co metal impurities. In Fig. 2(c,d), the conditions were similar to those in Fig. 2b, the peak patterns and relative intensities of Co 2p matched well with the XPS spectra of well-characterized CoO standards in the literature, further demonstrating that these particles were CoO. [6, 33] The ICP analysis results for C350, C400, C500 and C600 hybrid nanocomposites are given in the Table S1. As shown in the table, the dissolved Co content of C600 is higher than that of C500 (or C350, C400). The result illustrates that CoO nanoparticles are reduced into metallic Co nanoparticles by carbon layers, along with the temperature increased from 500^{o}C to 600^{o}C and the conductive carbon layers were converted from the OA^{-} carbonization.

Fig. 3(a-c) shows the TEM images of the CoO/C nanocomposites, which demonstrated the CoO nanoparticles densely wrapped by the carbon layer almost without aggregation. It can be seen that C350 sample (Fig. 3a) was

assembled by attaching ultra-small CoO nanoparticles (~ 3.0 nm in diameter) with a high density on a carbon nanosheet (Fig. 3d). The carbon layers are relatively thick, and the CoO nanoparticles occupied in close-packed arrangement on the surface of the carbon layer. It clearly revealed that with the temperature increased, the carbon layer became thinner and uneven and the uniform CoO nanoparticles with a high density were homogeneously wrapped by the carbon layers (Fig. 3(b, c)). These results agree well with the SEM images, as shown in (Fig. S3). Moreover, the size of a single CoO nanoparticle is about 5.4 nm for C400 (Fig. 3e) and 6.1 nm for C500 (Fig. 3f). HRTEM images (Fig. 3e and 3f) of the nanoparticles display the regular lattice (with the interplanar spacing of 0.21 nm), which is well assigned to (200) crystal plane of CoO, further demonstrating that the nanoparticles are CoO. The formation of these different structure may be attributed to the dehydration, carbonization and decomposition of $Co(OH)_2$@OA during annealing in Ar atmosphere.[38]

3.4. Electrochemical performance of CoO/C nanocomposites

Fig. 4(a, c, e) give the typical charge/discharge voltage profiles of the CoO/C nanocomposites at a current density of 70 mA g^{-1} in a potential range of 0.01-3 V. It can be seen that the initial discharge capacities for C350, C400 and C500 nanocomposites are 1018.1, 1139.1 and 1618.2 mA h g^{-1} and charge capacities of 522.9, 663.2, 829.9 mA h g^{-1}, leading to an initial Coulombic efficiency of 51.4%, 58.2% and 51.3%, respectively. The relatively low initial Coulombic efficiency may be caused by the irreversible capacity loss, including

inevitable formation of SEI and decomposition of electrolyte, which are common to most transition-metal oxide anode materials.[39-41] Furthermore, their Coulombic efficiency rapidly increased from 51%, 58% and 51% for the first cycle to about 99% after three cycles and remains nearly 100%, which suggested a facile lithium insertion/extraction associated with efficient transport of ions and electrons in the electrodes. During the 1st discharge process, the plateau at about 0.7 V corresponds to the reduction of CoO and the formation of Li_2O. This plateau becomes weak in the following cycles which are similar to previous reports about CoO/C composites because of the combinative electrochemical behavior of CoO and carbon.[31, 42] In the charge process, two plateaus at about 1.25 and 2.0 V could be assigned to the delithiation of carbon and the oxidation of Co to CoO. The irreversible, large capacity loss arising in the initial cycles may be assigned to the interfacial Li storage[12] or the reversible growth of a polymeric gel-like film resulting from the kinetically activated electrolyte degradation.

Fig. 4(b, d, f) present the cycling performance of the CoO/C at a current density of 70 mA g^{-1} between the potential of 0.01-3 V (vs. Li^+/Li). As shown in Fig. 2b, from the 10th cycle onwards, the C350 gives a more stable capacity at around 300 mA h g^{-1} and shows good cyclic retention during the 50 charge/discharge cycles, which suggested a facile lithium insertion/ extraction associated with efficient transport of ions and electrons in the electrodes. It should be emphasized that the reversible capacities of the C400 and C500 after

25th cycle are arising from 481.9 and 450.4 mA h g^{-1} to 640.3, 642.1 mA h g^{-1} after 50 discharge/charge cycles (Fig. 4(d, f)). A similar phenomenon was widely observed in the previously reported metal oxide/graphene composites.[12, 42] The reason can be explained that the in-situ generated cobalt metal nanocrystals during lithium-insertion processes can serve as efficient catalysts to activate the reversible formation and decomposition of SEI components and the polymeric gel-like films on the active particles. [46-48] The enhanced cycling performance of CoO/C nanocomposites could be attributed to the presence of the thin carbon layer around the CoO nanoparticles, which prevent the adjacent nanoparticles from contacting each other directly and therefore minimizes the aggregation of the nanoparticles in the charge-discharge process. The similar performance was widely observed in the previously reported transition metal oxide/carbon nanocomposites.[43-45]

The excellent electrochemical properties of the CoO/C nanocomposites could be attributed to the following factors. First, the small size of the CoO nanoparticles anchored onto the carbon layer, which ensure the electrodes maintain their integrity over many charge/discharge cycles and shortens the transport path for both electrons and lithium ions. The absolute volume change of each single CoO nanoparticles was small and thus the small size is hard to preconceive their further reduction, which is beneficial for preserving electrical contact between the active nanoparticles and conductive carbon layer. Second, the uniform and continuous carbon layers between CoO nanoparticles not only

remarkably enhance the electrical conductivity, but also facilitate the electron transfer on the electrode/electrolyte interfaces and accommodate the volume change of CoO nanoparticles during the discharge/charge cycling.

3.5. Characterization of Co/C nanocomposites

The TEM image (Fig. 5a) of sample C600 revealed that the Co nanoparticles are uniformly dispersed on the carbon nanosheets with a size of about 15 nm. The structure of the sample can be further revealed by the corresponding SEM image (Fig. S4a). Fig. 5b presents the charge/discharge profiles of the C600 in the 1st, 25th, 50th cycles at a current density of 70 mA g^{-1}. In the first cycle, the discharge curve of C600 had a flat potential plateau at about 1.2 V, followed by a sloping potential at about 0.8 V. From the second cycle onward, the charge/discharge curves are tending toward stability, implying good cycling property, which is also illustrated in the CV curves (Fig. 5c). This may be due to the carbon layers, which improved the electrical conductivity and the contact area of the electrode and electrolyte, further leading to the increasing utilization of the active material. Fig. 5c show the CV curves of the first three cycles of C600. There are two distinctive reduction peaks at 0.75 and 1.2 V in the first cathodic scan, without obvious decline and shift to higher voltage area in the following cycles indicating good capacity retention of Co/C composite electrode. The cathodic peak at 1.25 V and the anodic peak at 2.2 V are derived from the reduction of Li and the regeneration of CoO. Fig. 5d shows the capacity retention properties of C600 at a current

density of 70 mA g^{-1}. Notably, the Co/C exhibits a higher reversible specific capacity of about 500 mA h g^{-1} after 10 cycles. These may because nano-sized Co facilitates the decomposition of Li_2O during the charging process, making the electrochemical reaction more reversible and resulting in a smaller capacity loss during cycling.

4. Conclusions

In summary, ultra-small CoO and Co nanoparticles embedded in 2-D carbon nanosheets (CoO/C and Co/C nanosheets) have been successfully fabricated by a facile molten salt method. When used as the electrode material for LIBs, the obtained CoO/C and Co/C nanocomposites exhibit the capacities of 642.1 and 500 mA h g^{-1} over 50 cycles at a current density of 70 mA g^{-1}. The carbon nanosheet can accommodate the strain, provide larger specific area and enhance the conductivity during the charge/discharge process, which is the responsible for the enhanced performance on electrochemical test. Moreover, the facile molten salt process makes it a promising route to design high performance of metal or metal oxides wrapped by carbon layers for the applications in practical energy storage and conversion devices.

Acknowledgements

This work was supported by National Natural Science Foundation of China (21566037, 51006046, 51172005) and NSFC-RGC Joint Research Scheme (51361165201).

Notes and references

† Electronic Supplementary Information (ESI) available: XRD pattern of $Co(OH)_2$@OA complex precursor, FT-IR and TGA curves of $Co(OH)_2$@OA, Detailed SEM images of CoO/C, High-magnification TEM images of CoO, ICP analysis of C350, C400, C500 and C600. See DOI: 10.1039/b000000x/

1. M. V. Reddy, G. Prithvi, K. P. Loh and B. V. Chowdari, *ACS Appl. Mater. Interfaces*, 2014, 6, 680-690.
2. C. Zhou, Y. Zhang, Y. Li and J. Liu, *Nano Lett.*, 2013, 13, 2078-2085.
3. B. Jang, M. Park, O. B. Chae, S. Park, Y. Kim, S. M. Oh, Y. Piao and T. Hyeon, *J. Am. Chem. Soc.*, 2012, 134, 15010-15015.
4. H. B. Wu, J. S. Chen, H. H. Hng and X. W. Lou, *Nanoscale*, 2012, 4, 2526-2542.
5. Y. Sun, X. Hu, W. Luo and Y. Huang, *J. Phys. Chem. C*, 2012, 116, 20794-20799.
6. M. Zhang, E. Uchaker, S. Hu, Q. Zhang, T. Wang, G. Cao and J. Li, *Nanoscale*, 2013, 5, 12342-12349.
7. L. Huang, D. Chen, Y. Ding, S. Feng, Z. L. Wang and M. Liu, *Nano letters*, 2013, 13, 3135-3139.
8. K. H. Seng, M. H. Park, Z. P. Guo, H. K. Liu and J. Cho, *Angew. Chem. Int. Ed.*, 2012, 51, 5657-5661.

9. B. Li, H. Cao, J. Shao, G. Li, M. Qu and G. Yin, *Inorg. Chem.*, 2011, 50, 1628-1632.
10. Y. Sun, X. Hu, W. Luo and Y. Huang, *J. Mater. Chem.*, 2012, 22, 13826-13831.
11. L. Zhao, Y. S. Hu, H. Li, Z. Wang and L. Chen, *Adv. Mater.*, 2011, 23, 1385-1388.
12. S. Xiong, J. S. Chen, X. W. Lou and H. C. Zeng, *Adv. Funct. Mater.*, 2012, 22, 861-871.
13. G. X. Pan, X. H. Xia, F. Cao, J. Chen, P. S. Tang, Y. J. Zhang and H. F. Chen, *Electrochim. Acta*, 2014, 133, 522-528.
14. X. Huang, J. Chen, H. Yu, R. Cai, S. Peng, Q. Yan and H. H. Hng, *J. Mater Chem. A*, 2013, 1, 6901-6907.
15. J. Wang, N. Yang, H. Tang, Z. Dong, Q. Jin, M. Yang, D. Kisailus, H. Zhao, Z. Tang and D. Wang, *Angew. Chem.*, 2013, 52, 6417-6420.
16. X. Zhou, Y. X. Yin, L. J. Wan and Y. G. Guo, *Chem. Commun.*, 2012, 48, 2198-2200.
17. H. Zhang, H. Tao, Y. Jiang, Z. Jiao, M. Wu and B. Zhao, *J. Power Sources*, 2010, 195, 2950-2955.
18. J. Yue, X. Zhao and D. Xia, *Electrochem. Commun.*, 2012, 18, 44-47.
19. L. Zhang, P. Hu, X. Zhao, R. Tian, R. Zou and D. Xia, *J. Mater. Chem. A.*, 2011, 21, 18279-18283.

20. C. Zhang, J. Chen, Y. Zeng, X. Rui, J. Zhu, W. Zhang, C. Xu, T. M. Lim, H. H. Hng and Q. Yan, *Nanoscale*, 2012, 4, 3718-3724.

21. J. Z. Wang, C. Zhong, D. Wexler, N. H. Idris, Z. X. Wang, L. Q. Chen and H. K. Liu, *Chem. Eur. J.*, 2011, 17, 661-667.

22. W. Yuan, J. Zhang, D. Xie, Z. Dong, Q. Su and G. Du, *Electrochim. Acta*, 2013, 108, 506-511.

23. H. Qiao, L. Xiao, Z. Zheng, H. Liu, F. Jia and L. Zhang, *J. Power Sources*, 2008, 185, 486-491.

24. Z. Yang, J. Shen and L. A. Archer, *J. Mater. Chem.*, 2011, 21, 11092-11097.

25. D. Lan, Y. Chen, P. Chen, X. Chen, X. Wu, X. Pu, Y. Zeng and Z. Zhu, *ACS Appl. Mater. Interfaces*, 2014, 6, 11839-11845.

26. M. Li, Y. X. Yin, C. Li, F. Zhang, L. J. Wan, S. Xu and D. G. Evans, *Chem. Commun.*, 2012, 48, 410-412.

27. Y. Piao, H. S. Kim, Y. E. Sung and T. Hyeon, *Chem. Commun.*, 2010, 46, 118-120.

28. K. Xie, P. Wu, Y. Zhou, Y. Ye, H. Wang, Y. Tang, Y. Zhou and T. Lu, *ACS applied materials & interfaces*, 2014, 6, 10602-10607.

29. Z. Niu, L. Liu, L. Zhang, Q. Shao, W. Zhou, X. Chen and S. Xie, *Adv. Mater.*, 2014, 26, 3681-3687.

30. Z. Zhang, L. Su, M. Yang, M. Hu, J. Bao, J. Wei and Z. Zhou, *Chem. Comm.*, 2014, 50, 776-778.

31. A. Riaz, K. N. Jung, W. Chang, S. B. Lee, T. H. Lim, S. J. Park, R. H. Song, S. Yoon, K. H. Shin and J. W. Lee, *Chem. Comm.*, 2013, 49, 5984-5986.

32. M. Zhang, F. Yan, X. Tang, Q. Li, T. Wang and G. Cao, *J. Mater. Chem. A.*, 2014, 2, 5890-5897.

33. F. D. Wu and Y. Wang, *J. Mater. Chem.*, 2011, 21, 6636-6641.

34. W. . Zhang, X. . Wu, J. . Hu, Y. . Guo and L. . Wan, *Adv. Funct. Mater.*, 2008, 18, 3941-3946.

35. J. H. Kim and Y. C. Kang, *Nanoscale*, 2014, 6, 4789-4795.

36. Y. J. Mai, X. L. Wang, J. Y. Xiang, Y. Q. Qiao, D. Zhang, C. D. Gu and J. P. Tu, *Electrochim. Acta*, 2011, 56, 2306-2311.

37. J. Liu, Y. Zhou, C. Liu, J. Wang, Y. Pan and D. Xue, *CrystEngComm*, 2012, 14, 2669-2674.

38. J. Liu and D. Xue, *Electrochimica Acta*, 2010, 56, 243-250.

39. N. Kang, J. H. Park, J. Choi, J. Jin, J. Chun, I. G. Jung, J. Jeong, J. G. Park, S. M. Lee, H. J. Kim and S. U. Son, *Angew. Chem.*, 2012, 51, 6626-6630.

40. X. Xu, R. Cao, S. Jeong and J. Cho, *Nano letters*, 2012, 12, 4988-4991.

41. I. T. Kim, A. Magasinski, K. Jacob, G. Yushin and R. Tannenbaum, *Carbon*, 2013, 52, 56-64.

42. F. Li, Q.-Q. Zou and Y.-Y. Xia, *Journal of Power Sources*, 2008, 177, 546-552.

43. Z. R. Dai, Z. W. Pan and Z. L. Wang, *Advanced Functional Materials*, 2003, 13, 9-24.

44. Y. Liu, C. Mi, L. Su and X. Zhang, *Electrochimica Acta*, 2008, 53, 2507-2513.

45. X. W. Lou, D. Deng, J. Y. Lee, J. Feng and L. A. Archer, Advanced materials, 2008, 20, 258-262.

46. J. W. Yin, H. M. Shi, P. Wu, Q. Y. Zhu, H. Wang, Y. W. Tang, Y. M. Zhou and T. H. Lu, New J. Chem. 2014, 38, 4036--4040.

47 L. W. Su, Z. Zhou, P. W. Shen, J. Phys. Chem. C, 2012,116, 23974-23980.

48 Q. Y. Zhu, P. Wu, J. J. Zhang, W. Y. Zhang, T. H. Lu, ChemSusChem, 2015, 8, 131-137.

Figures and figure captions

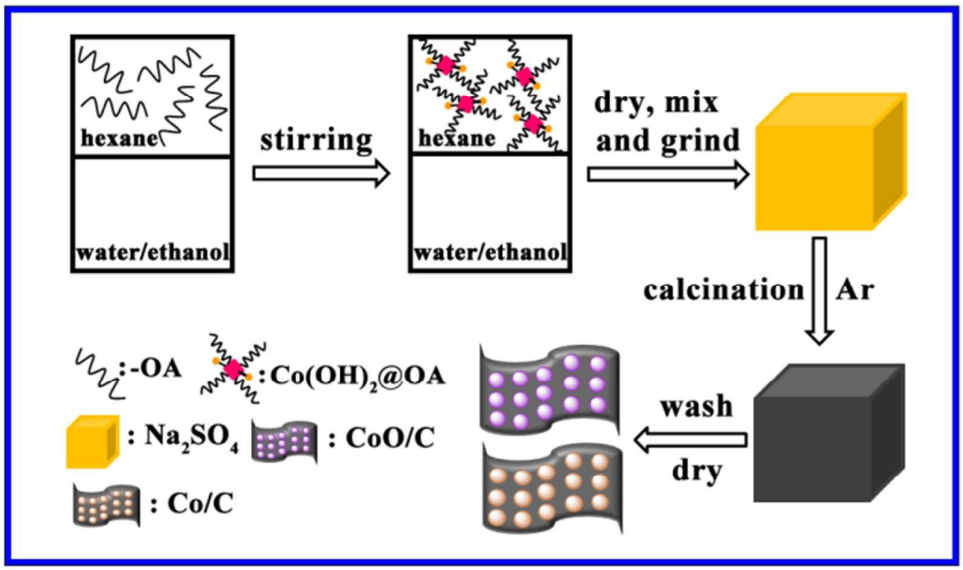

Scheme 1 Schematic illustration of the synthesis path of CoO/C nanocomposites or Co/C nanocomposites.

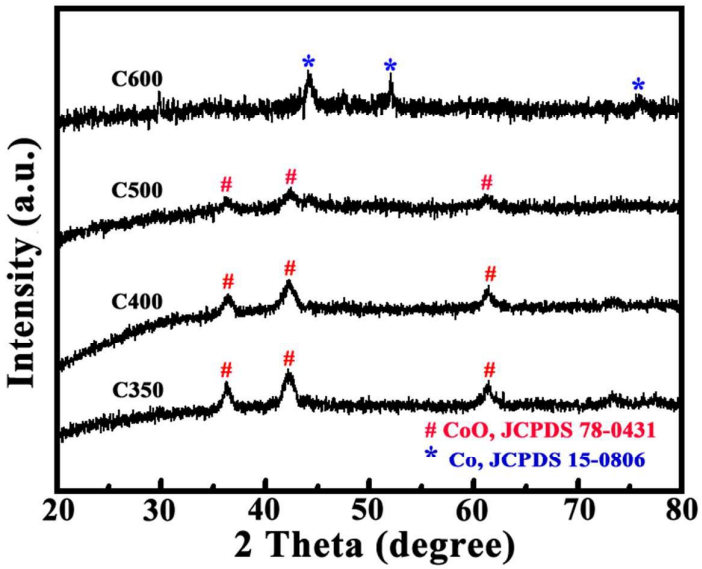

Fig. 1 XRD patterns of the CoO/C nanocomposites and Co/C nanocomposites prepared at 350, 400, 500 and 600°C (C350, C400, C500 and C600).

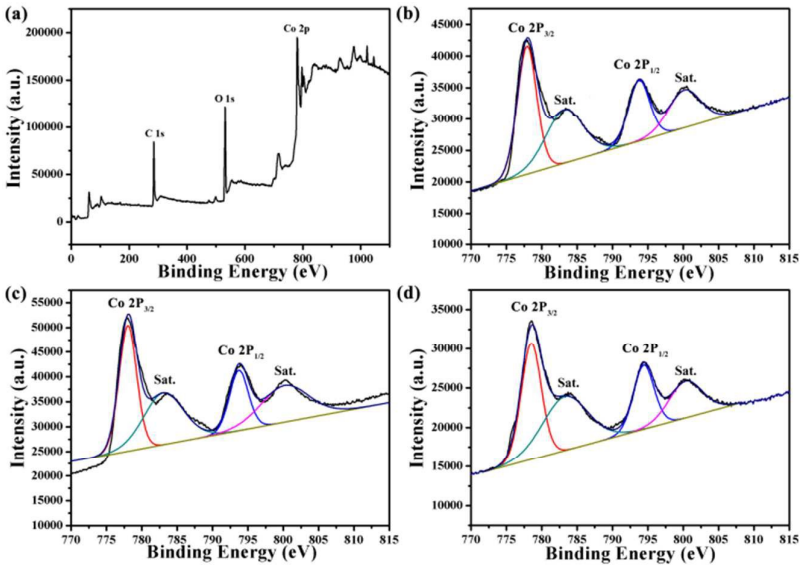

Fig. 2 XPS spectra of (a) full scan survey (C400) and (b-d) Co 2p for CoO nanocomposites (C350, C400, C500).

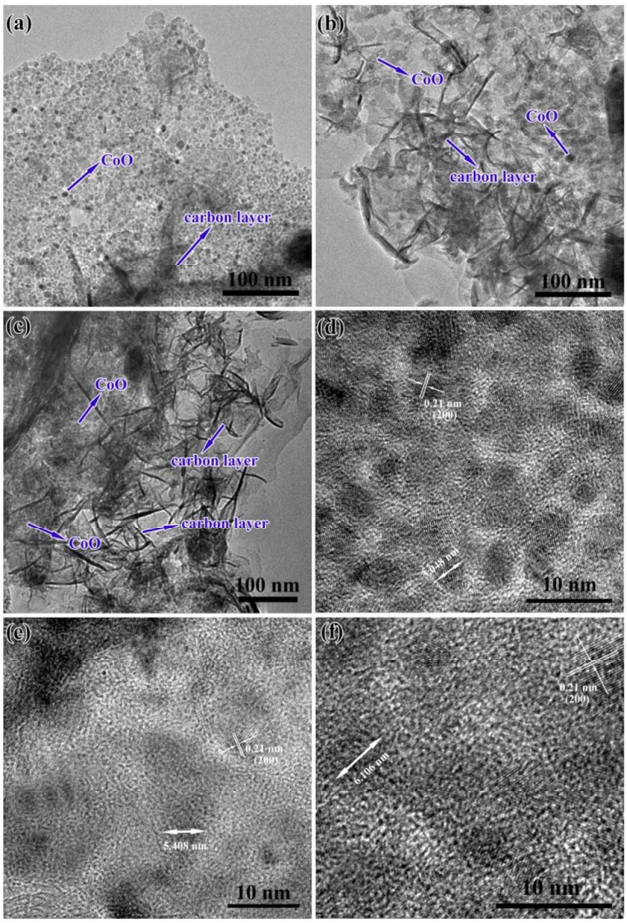

Fig. 3 (a-c) TEM images of the as-prepared CoO/C nanocomposites prepared at 350°C,

400°C, 500°C (C350, C400, C500); (d-f) HR-TEM images of CoO/C (C350, C400, C500) nanocomposites.

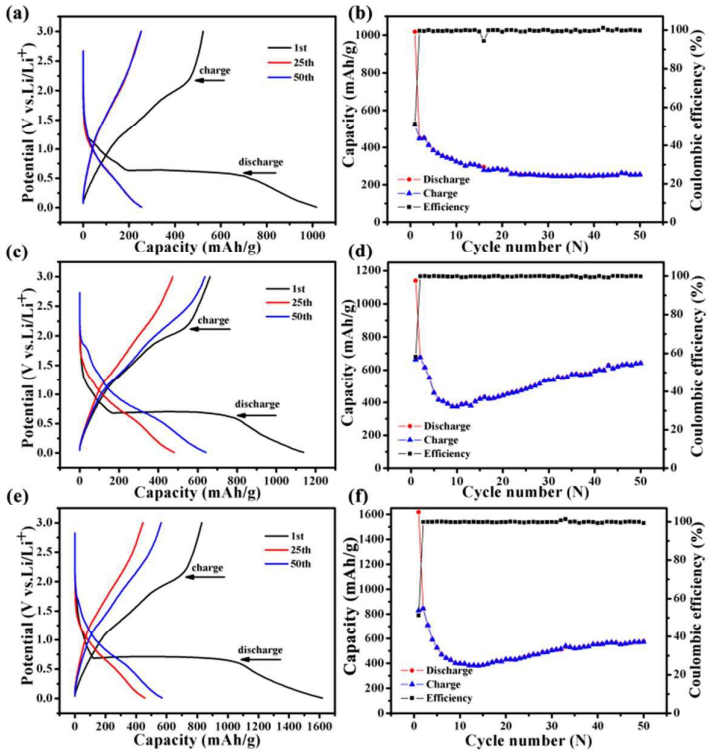

Fig. 4 (a, c, e) Typical charge/discharge curves of C350, C400, C500 samples in the voltage range of 0.01-3.0 V at a current density of 70 mA g^{-1}; (b, d, f) Cyclic performance of C350, C400, C500 samples in the voltage range of 0.01-3.0 V at a current density of 70 mA g^{-1}.

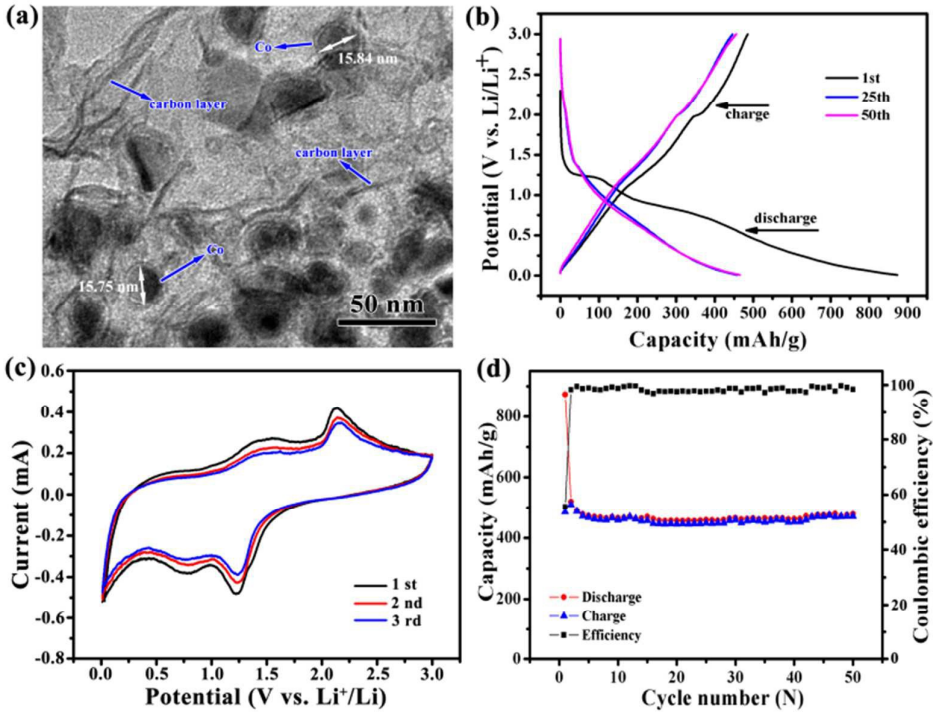

Fig. 5 (a) TEM image of C600; (b) Typical charge/discharge curves of C600 sample in the voltage range of 0.01-3.0 V at a current density of 70 mA g^{-1}; (c) CV curves of C600 sample obtained at a voltage range of 0.0 to 3.0 V (vs Li^+/Li) and a scan rate of 0.1 mV/s; (d) Cyclic performance of C600 sample in the voltage range of 0.01-3.0 V at a current density of 70 mA g^{-1}.

Graphical abstract

A simple procedure for the preparation of CoO and Co nanoparticles and using Na_2SO_4 as the template for the small nanoparticles encapsulated with thin carbon layers.